ACS APPLIED ENERGY MATERIALS

www.acsaem.org Letter

A Type I Heterointerface between Amorphous PbI_2 Overlayers on Crystalline $CsPbI_3$

Thomas W. Kasel and Christopher H. Hendon*

Cite This: *ACS Appl. Energy Mater.* 2020, 3, 10328−10332 Read Online

ACCESS | Metrics & More | Article Recommendations | Supporting Information

ABSTRACT: PbI_2, an insulating byproduct formed from lead halide perovskite decomposition, is thought to pose issues for implementation of these materials in photovoltaic applications. Here, we examine the electronic properties of amorphous PbI_2 overlayers on the $CsPbI_3^-$ model perovskite. Using a combination of molecular dynamics and density functional theory, we report that α-PbI_2 does not introduce midgap states between the $CsPbI_3$ band extrema; instead, it brackets the frontier bands of the bulk $CsPbI_3$ lattice forming a type I heterointerface. While this overlayer may be detrimental to solar devices, it offers a unique opportunity to form heterogeneous nanocrystals, akin to strategies employed for other binary semiconductors (e.g., PbSe nanocrystals coated in wider gap PbS).

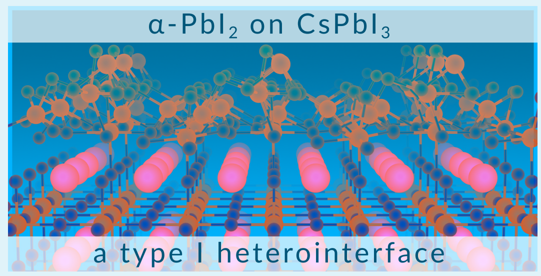

KEYWORDS: *amorphous lead iodide, perovskite, cesium lead iodide, density functional theory, ab initio molecular dynamics*

The narrow band gap and large band dispersion of Pb-based perovskites make them intriguing candidates for cheap photovoltaic technologies.[1,2] The same electronic properties also enable a wide gamut of colloidal nanocrystals:[3] the champion materials in both cases are composed of PbI_3^- with an additional monovalent cation contained within the lattice. While one of the attractions of this class of materials is their ease of synthesis, the maturation of the field has revealed several chemical instabilities that limit the widespread implementation in technologies, particularly in photovoltaic applications. The most concerning of these is the decomposition of the crystalline lattice in the presence of moisture, a process thought to proceed via a Brønsted acid-catalyzed protonation of I^-.[4−11] Furthermore, in the increasingly popular organic iodide plumbates, the lattices often contain weakly acidic protons at the A-site (e.g., $CH_3NH_3^+$, $pK_a = 10.6$). While these cations have led to champion photovoltaic efficiencies,[12] they are intrinsically more reactive than their Cs^+ counterparts as the ammonium protons further interact with the scaffold I^- via secondary bonding (e.g., hydrogen bonding).[13−17] Beyond being a byproduct of Brønsted acid decomposition, PbI_2 has also been shown to form in protic A-site perovskites via oxidation in air:

$$2(CH_3NH_3)PbI_3 + \frac{1}{2}O_2 \rightarrow 2CH_3NH_2 + 2PbI_2 + I_2 + H_2O$$

In this case, the reaction is thought to proceed via the entropic propensity to form several gaseous products.[18] In all cases, protonation of the bridging iodides promotes the formation of PbI_2 (the thermodynamic product), a process readily observed by a color change from the black PbI_3^- lattice to the characteristic yellow of PbI_2.[17,19] Furthermore, the yellow discoloration has been observed at low temperature, and the PXRD data presented by Wang et al. suggests that the PbI_2 layering is likely composed of locally disordered/amorphous PbI_2 sheets, as evidenced by the broad reflections assigned to (001) and no clear evidence of other in-plane reflections.[20]

In order to simplify our model by excluding the orientation dependence of the methylammonium cation, and its potential to deprotonate in our ab initio molecular dynamics simulations, we elected to perform the following study on $CsPbI_3$ as a representative PbI_3^--based material. By extension, we suspect the findings in this paper likely apply to other perovskites. Electronic structure calculations of bulk PbI_2 and $CsPbI_3$, Figure 1, suggest that the formation of PbI_2 on the surface of a lead iodide perovskite is hypothesized to have two primary effects on bulk material properties: (i) the installation of shallow midgap trap states in the valence band and (ii) the widening of the band gap, diminishing the ability to extract charges from its surface. Hence, the emergence of PbI_2 is largely believed to be detrimental at both grain boundaries and at material surface contacts in photovoltaic devices. There is, however, some evidence that the presence of PbI_2 may be beneficial, as Kim et al. demonstrated that the existence of

Received: August 31, 2020
Accepted: October 13, 2020
Published: October 19, 2020

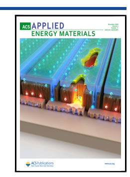

https://dx.doi.org/10.1021/acsaem.0c02122
ACS Appl. Energy Mater. 2020, 3, 10328−10332

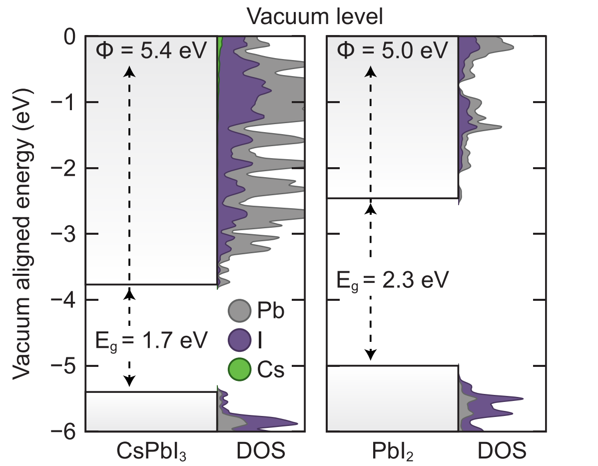

Figure 1. Band edge diagram for $CsPbI_3$ and PbI_2. The VBM of PbI_2 lies within the gap of $CsPbI_3$ suggesting that its existence results in midgap states. The work function for $CsPbI_3$ was obtained from the literature.[21]

excess PbI_2 boosts device performance.[22] Others have suggested that the presence of excess PbI_2 acts more like a double-edged sword such that small amounts of excess PbI_2 increases device efficiency;[23,24] they demonstrate that excess PbI_2 simultaneously decreases device stability. As such, there is currently a debate as to whether excess PbI_2 should be explicitly avoided, or whether the formation of trace amounts of excess PbI_2 should be welcomed; it is difficult to know what to make of it.

Our initial results seem to suggest that PbI_2 may not affect the conduction band, and hence electron mobility, but our simple band alignment image is insufficient to validate our former concern as the electronic properties of the $PbI_2/CsPbI_3$ heterostructure will have dissimilar electronic properties as compared to the bulk alignments, primarily due to band bending and redistribution of electrons. The alignment presented in Figure 1, however, provides an indication that the wider band gap will likely result in an Ohmic interfacial layer with the underlaying PbI_3^- layers.

In addition to pondering the effect on photovoltaic properties, and being motivated by our initial band alignement, we began to think about opportunities for using PbI_2 overlayers as a novel route to forming supported nanocrystals as a functional result of lattice degradation. While this overlaying approach has been recently demonstrated for lead oxide overlayers, albeit not for nanocrystal formation explicitly,[25] the appeal of using PbI_2 formed by simple exposure to air offers a unique avenue to create novel crystal morphologies. Furthermore, our band alignment prediction suggests that, depending on the extent of energetic reordering arising from the interface, PbI_2 overlayers could act much the same as the PbO_x overlayer, or analogous to PbS coatings on PbSe nanocrystals.[26,27] This would afford numerous new opportunities for formation of $PbI_2/APbI_3$ hybrids. By inducing natural lattice degradation processes, a core@shell architecture could be readily generated. In this regard, the intensely studied degradation of perovskite lattices could provide a utility, rather than a persistent problem. Of course, these overlayers are only useful if the surface states do not contribute to the valence and conduction band edges. In photovoltaics, such surface state contribution could act as a charge carrier trap, likely lowering photovoltaic performance. For core@shell architectures, these band edge states would likely interfere with luminescent properties. It is therefor paramount that the location of PbI_2 states relative to a pristine PbI_3^- lattice be elucidated. To make this assessment, we turned to more complicated models: amorphous lead iodide (α-PbI_2) overlayers on crystalline $CsPbI_3$ (i.e., α-PbI_2@$CsPbI_3$).

Using the approach discussed in the Computational Methods section, we constructed surface models of both pristine and disordered PbI_2 and $CsPbI_3$, as well as several geometrically dissimilar models of α-PbI_2@$CsPbI_3$. The latter were generated using a combined ab initio molecular dynamics simulation. All structures were then subject to a hybrid DFT single point to obtain a higher fidelity electronic structure, providing quantitative information about the electronic structure at the interfacial heterostructure models, Figure 2a. Notably, the reduction in the $CsPbI_3$ band gap shown in Figure 2b can be attributed to the increasing valence band energy associated with the dangling surface I^-. These I^- arise from reducing the system to two-dimensionality, and passivating the surface with checkerboard like undercoordinated bonds to minimize artificial surface dipoles.

Along the same lines, we hypothesized that the disorder of amorphous PbI_2 would exhibit an increase in valence band energy compared to crystalline 2D PbI_2, which is 8 kcal/formula unit more stable than its amorphous surface analogue because it features fewer undercoordinated iodides (see Supporting Information structures for a geometric comparison). The disorder, however, limits our ability to rigorously align the model to an internal vacuum level, as an artificial dipole is installed across the void space. Hence, the band alignment of amorphous PbI_2 containing models using absolute references such as those in Figure 1 would provide a "worst case scenario". As such, we elected to instead align to the PbI_3^- lattice as (i) by definition electronic states can be compared across models with the assumption that deep-core PbI_3^- is identical across all models, and (ii) the extent and importance of perturbations caused by amorphous PbI_2 is drawn directly through comparison with the PbI_3^- lattice. By using an external reference, and aligning our models to the valence band maximum (which we refer to as the "Fermi level" in our undoped, temperature independent models), we are able to draw the alignment shown in Figure 2b. It should be noted that all of our dissimilar structures had similar features: (i) surface PbI_2 favored the formation of octahedral Pb, (ii) surface unsaturated iodides preferentially formed as many bonds as possible with surface Pb, and (iii) the interface between the crystalline regions and the amorphous regions are incoherent.

Running our models in quadruplicate (to account for any anomalies and rare events possibly generated in a single ab initio molecular dynamics simulation), we find that, contrary to Figure 1, no midgap states were introduced by overlayer α-PbI_2. By examination of both the orbital projection of the valence and conduction bands (Figure 2a), the surface iodides do not contribute to the frontier bands. Furthermore, with a comparison of slab models of both amorphous PbI_2 and $CsPbI_3$, Figure 2b, the surface overlayers appear to bracket both the valence and conduction bands of the intact perovskite (in essence, a type I heterojunction). In photovoltaic applications, this installs a difficult to surmount energy barrier for charge carriers, likely reducing the photovoltaic performance of the absorbing layer. As such, if a PbI_2 region exists

https://dx.doi.org/10.1021/acsaem.0c02122
ACS Appl. Energy Mater. 2020, 3, 10328−10332

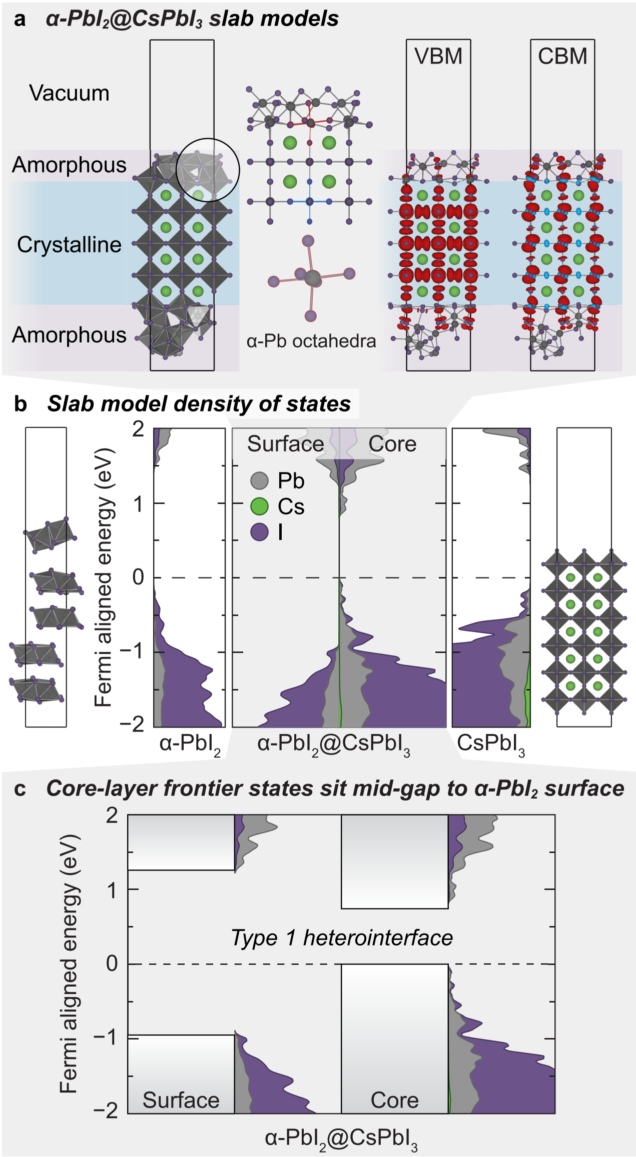

Figure 2. (a) Models used to recover the electronic effects of the decomposition of a pristine PbI_3^- lattice to α-PbI_2. (b) α-PbI_2@$CsPbI_3$ and its charge density calculated at the valence band maximum and conduction band minimum. Charge densities were plotted with an isosurface value of 10^{-5} e^- Å^3. (c) Fermi aligned densities of states were calculated using HSE06sol+SOC (PBEsol +43% Hartree−Fock exchange + spin−orbit coupling). The α-PbI_2 region has a ~950 and a ~1250 meV energy barrier associated with hole transport and electron transport from the core to the surface, respectively. Here, the Fermi level is defined as the valence band maximum, because the computations are performed on an undoped, temperature independent semiconductor.

between the location of charge carrier generation and their corresponding transport layers, it is likely that photovoltaic performance will be diminished. However, this alignment is similar to those found for PbS@PbSe, as well as for the PbO_x@perovskite architectures, suggesting that the overlayers could prolong exciton lifetimes: Thus, could α-PbI_2 be a useful overlayer in forming metastable nanoparticles?

While we cannot be conclusive in our assessment, the density of states plots provide some reasons to be optimistic. The density of states plot of α-PbI_2@$CsPbI_3$ in Figure 2c reveals that the highest energy occupied α-PbI_2 state occurs ~0.95 eV below the Fermi level. Similarly, the first unoccupied α-PbI_2 state appears ~1.25 eV above the Fermi level. Also, our amorphous layer pseudogap aligns nicely with the observed yellow color seen in experiments. However, the lack of α-PbI_2 states within the band gap, or defining the band edges, indicates that α-PbI_2 does not result in the midgap states predicted in Figure 1. Hence, we suggest that only when the ratio between the interfacial surface area and the bulk volume increases (i.e., very large surface area and low bulk volume) will these frontier α-PbI_2 states have an observable effect on pristine bulk frontier band properties. Further, the interfacial charge density does not appear to alter the chemistry of the subsurface $CsPbI_3$, implying that the thickness of the amorphous region has little to no influence on the frontier electrical properties of the bulk. This suggests that the location of PbI_2 regions has a larger impact on photovoltaic performance than its size. However, we reiterate that photovoltaic performance is likely to be inhibited only if PbI_2 regions occur between the location of charge carrier generation and their corresponding transport materials. It is not clear from our model, however, how PbI_2 could be beneficial to device performance, and further effort is required to understand that effect.

From the arguments above, we interpret these data to suggest that the addition of amorphous PbI_2 on the surface of $CsPbI_3$ does not result in midgap states predicted from simpler bulk band edge alignments of their respective bulk crystalline models. Our DFT calculations indicate that α-PbI_2 overlayers on crystalline $CsPbI_3$ generate a type I semiconductor heterointerface, which ultimately does not affect the electronic properties afforded by the frontier states in $CsPbI_3$. In this regard, techniques to induce lattice degradation could be utilized postsynthetically as a novel and simple path for generating perovskite core@shell architectures, where crystallite size could be kinetically controlled by exposure time to water or another PbI_2 forming mechanism. Additionally, since the charge density of the models suggests that the thickness of the α-PbI_2 shell has little impact on the electronics of the core, the extent of surface passivation as well as the quantum confinement experienced by the core could readily be tuned by the extent of degradation induced postsynthetically. While these results are detrimental from a photovoltaic sense (if they prevent contact between the underlaying perovskite and the charge extracting layers), we suspect that there are several opportunities for encapsulated perovskite nanoparticles formed from controlled decomposition of PbI_3^- lattices containing monovalent cations.

■ COMPUTATIONAL METHODS

Geometric optimizations were performed on α-PbI_2@$CsPbI_3$, PbI_2, and $CsPbI_3$ using a 500 eV planewave cutoff, a projector-augmented-wave (PAW) basis, and a $2 \times 2 \times 1$, a $4 \times 4 \times 1$, and a $2 \times 2 \times 1$ k-grid, respectively. Densities of states and charge densities were recovered using HSE06sol+SOC (PBEsol +43% Hartree−Fock exchange + spin−orbit coupling).[28] All calculations were performed using the Vienna ab initio Simulation Package (VASP).[29] Slabs were constructed from the geometrically equilibrated bulk unit cell of $CsPbI_3$. To do so, the cell was expanded to a $2 \times 2 \times 8$ supercell, and 17.5 Å of vacuum was added. To create the α-PbI_2@$CsPbI_3$ system, half of the PbI_3^- lattice was stoichiometrically exchanged for PbI_2 by removal of equal amounts of Cs and I. The cell was thus composed of half $CsPbI_3$ and half PbI_2 in a 2−4−2 (PbI_2−$CsPbI_3$−PbI_2) configuration. For all calculations using this model, the atomic

https://dx.doi.org/10.1021/acsaem.0c02122
ACS Appl. Energy Mater. 2020, 3, 10328−10332

coordinates of core $CsPbI_3$ were held constant (frozen) to provide a constant accurate description of a core $CsPbI_3$ lattice. The $CsPbI_3$ slab was created through a 2 × 2 × 6 supercell expansion, and a vacuum of approximately 30 Å was added to match the c lattice vector of α-PbI_2@$CsPbI_3$. To model a slab of α-PbI_2, the optimized bulk of PbI_2 was expanded in a 1 × 1 × 5 supercell expansion, and 20 Å of vacuum was added.

Ab initio molecular dynamics simulations were then performed on α-PbI_2@$CsPbI_3$ and PbI_2 using a canonical ensemble (NVT) based upon the Nosé−Hoover thermostat.[30] α-PbI_2@$CsPbI_3$ was heated to 600 K at 1 K/fs and then rapidly cooled and held at 300 K for 10 ps, to trap a high energy α-PbI_2 surface. PbI_2 was heated to 500 K in 1 K/fs to simulate melting. In order to obtain statistical variability, all simulations of the α-PbI_2@$CsPbI_3$ model were run in quadruplicate. Interfacial lead and iodide were treated as part of the core as they mostly retained their octahedral geometry and only exhibited a slight distortion, as shown in Figure 2a.

■ ASSOCIATED CONTENT

Supporting Information

The Supporting Information is available free of charge at https://pubs.acs.org/doi/10.1021/acsaem.0c02122.

> Geometry files for bulk crystalline $CsPbI_3$ and PbI_2, crystalline and amorphous surfaces thereof, and quadruplicate surfaces of the heterostructures (ZIP)

■ AUTHOR INFORMATION

Corresponding Author

Christopher H. Hendon − *Department of Chemistry and Biochemistry, University of Oregon, Eugene, Oregon 97403, United States;* orcid.org/0000-0002-7132-768X; Email: chendon@uoregon.edu

Author

Thomas W. Kasel − *Department of Chemistry and Biochemistry, University of Oregon, Eugene, Oregon 97403, United States*

Complete contact information is available at: https://pubs.acs.org/10.1021/acsaem.0c02122

Notes

The authors declare no competing financial interest.

■ ACKNOWLEDGMENTS

Computational studies were performed using the High-Performance Computing cluster at the University of Oregon (Talapas), the Extreme Science and Engineering Discovery Environment (XSEDE) which is supported by National Science Foundation Grant ACI-1548562, and the Portland State University machine, Coeus, which is supported by the NSF (DMS1624776). C.H.H. was supported in part by the National Science Foundation under Grant DMR-1956403.

■ REFERENCES

(1) Kojima, A.; Teshima, K.; Shirai, Y.; Miyasaka, T. Organometal Halide Perovskites as Visible-Light Sensitizers for Photovoltaic Cells. *J. Am. Chem. Soc.* **2009**, *131*, 6050−6051.

(2) Natonal Renewable Energy Labratory. *Best Research-Cell Efficiency Chart*; 2019; https://www.nrel.gov/pv/cell-efficiency.html.

(3) Protesescu, L.; Yakunin, S.; Bodnarchuk, M. I.; Krieg, F.; Caputo, R.; Hendon, C. H.; Yang, R. X.; Walsh, A.; Kovalenko, M. V. Nanocrystals of Cesium Lead Halide Perovskites ($CsPbX_3$, X = Cl, Br, and I): Novel Optoelectronic Materials Showing Bright Emission with Wide Color Gamut. *Nano Lett.* **2015**, *15*, 3692−3696.

(4) Wang, R.; Xue, J.; Wang, K.-L.; Wang, Z.-K.; Luo, Y.; Fenning, D.; Xu, G.; Nuryyeva, S.; Huang, T.; Zhao, Y.; Yang, J. L.; Zhu, J.; Wang, M.; Tan, S.; Yavuz, I.; Houk, K. N.; Yang, Y. Constructive molecular configurations for surface-defect passivation of perovskite photovoltaics. *Science* **2019**, *366*, 1509−1513.

(5) Xiao, Z.; Bi, C.; Shao, Y.; Dong, Q.; Wang, Q.; Yuan, Y.; Wang, C.; Gao, Y.; Huang, J. Efficient, high yield perovskite photovoltaic devices grown by interdiffusion of solution-processed precursor stacking layers. *Energy Environ. Sci.* **2014**, *7*, 2619−2623.

(6) Wang, Z.; Lin, Q.; Chmiel, F. P.; Sakai, N.; Herz, L. M.; Snaith, H. J. Efficient ambient-air-stable solar cells with 2D-3D heterostructured butylammonium-caesium-formamidinium lead halide perovskites. *Nat. Energy* **2017**, *2*, 17135.

(7) Zheng, X.; Chen, B.; Dai, J.; Fang, Y.; Bai, Y.; Lin, Y.; Wei, H.; Zeng, X. C.; Huang, J. Defect passivation in hybrid perovskite solar cells using quaternary ammonium halide anions and cations. *Nat. Energy* **2017**, *2*, 17102.

(8) Wu, Y.; Xie, F.; Chen, H.; Yang, X.; Su, H.; Cai, M.; Zhou, Z.; Noda, T.; Han, L. Thermally Stable $MAPbI_3$ Perovskite Solar Cells with Efficiency of 19.19% and Area over 1 cm^2 achieved by Additive Engineering. *Adv. Mater.* **2017**, *29*, 1701073.

(9) Eperon, G. E.; Stranks, S. D.; Menelaou, C.; Johnston, M. B.; Herz, L. M.; Snaith, H. J. Formamidinium lead trihalide: a broadly tunable perovskite for efficient planar heterojunction solar cells. *Energy Environ. Sci.* **2014**, *7*, 982−988.

(10) Nie, W.; Tsai, H.; Asadpour, R.; Blancon, J.-C.; Neukirch, A. J.; Gupta, G.; Crochet, J. J.; Chhowalla, M.; Tretiak, S.; Alam, M. A.; Wang, H.-L.; Mohite, A. D. High-efficiency solution-processed perovskite solar cells with millimeter-scale grains. *Science* **2015**, *347*, 522−525.

(11) Yang, W. S.; Park, B.-W.; Jung, E. H.; Jeon, N. J.; Kim, Y. C.; Lee, D. U.; Shin, S. S.; Seo, J.; Kim, E. K.; Noh, J. H.; Seok, S. I. Iodide management in formamidinium-lead-halide-based perovskite layers for efficient solar cells. *Science* **2017**, *356*, 1376−1379.

(12) Amat, A.; Mosconi, E.; Ronca, E.; Quarti, C.; Umari, P.; Nazeeruddin, M. K.; Grätzel, M.; De Angelis, F. Cation-Induced Band-Gap Tuning in Organohalide Perovskites: Interplay of Spin-Orbit Coupling and Octahedra Tilting. *Nano Lett.* **2014**, *14*, 3608−3616.

(13) Zong, Y.; Zhou, Y.; Ju, M.; Garces, H. F.; Krause, A. R.; Ji, F.; Cui, G.; Zeng, X. C.; Padture, N. P.; Pang, S. Thin-Film Transformation of NH_4PbI_3 to $CH_3NH_3PbI_3$ Perovskite: A Methylamine-Induced Conversion-Healing Process. *Angew. Chem., Int. Ed.* **2016**, *55*, 14723−14947.

(14) Leguy, A. M. A.; Hu, Y.; Campoy-Quiles, M.; Alonso, M. I.; Weber, O. J.; Azarhoosh, P.; van Schilfgaarde, M.; Weller, M. T.; Bein, T.; Nelson, J.; Docampo, P.; Barnes, P. R. F. Reversible Hydration of $CH_3NH_3PbI_3$ in Films, Single Crystals, and Solar Cells. *Chem. Mater.* **2015**, *27*, 3397−3407.

(15) Christians, J. A.; Miranda Herrera, P. A.; Kamat, P. V. Transformation of the Excited State and Photovoltaic Efficiency of $CH_3NH_3PbI_3$ Perovskite upon Controlled Exposure to Humidified Air. *J. Am. Chem. Soc.* **2015**, *137*, 1530−1538.

(16) Yang, J.; Siempelkamp, B. D.; Liu, D.; Kelly, T. L. Investigation of $CH_3NH_3PbI_3$ Degradation Rates and Mechanisms in Controlled Humidity Environments Using in Situ Techniques. *ACS Nano* **2015**, *9*, 1955−1963.

(17) Song, Z.; Abate, A.; Watthage, S. C.; Liyanage, G. K.; Phillips, A. B.; Steiner, U.; Graetzel, M.; Heben, M. J. Perovskite Solar Cell Stability in Humid Air: Partially Reversible Phase Transitions in the PbI_2-CH_3NH_3-H_2O System. *Adv. Energy Mater.* **2016**, *6*, 1600846.

(18) Aristidou, N.; Eames, C.; Sanchez-Molina, I.; Bu, X.; Kosco, J.; Islam, M. S.; Haque, S. A. Fast oxygen diffusion and iodide defects mediate oxygen-induced degradation of perovskite solar cells. *Nat. Commun.* **2017**, *8*, 15218.

(19) Zhao, L.; Kerner, R. A.; Xiao, Z.; Lin, Y. L.; Lee, K. M.; Schwartz, J.; Rand, B. P. Redox Chemistry Dominates the Degradation and Decomposition of Metal Halide Perovskite Optoelectronic Devices. *ACS Energy Lett.* **2016**, *1*, 595−602.

https://dx.doi.org/10.1021/acsaem.0c02122
ACS Appl. Energy Mater. 2020, 3, 10328−10332

(20) Wang, S.; Yu, W.; Zhang, L.; Yang, Y. Crystallization process of PbI_2 solution in two-step deposition of $CH_3NH_3PbI_3$ for high-performance perovskite solar cells. *Sol. Energy Mater. Sol. Cells* **2017**, *161*, 444−448.

(21) Ravi, V. K.; Markad, G. B.; Nag, A. Band Edge Energies and Excitonic Transition Probabilities of Colloidal $CsPbX_3$ (X = Cl, Br, I) Perovskite Nanocrystals. *ACS Energy Lett.* **2016**, *1*, 665−671.

(22) Kim, Y. C.; Jeon, N. J.; Noh, J. H.; Yang, W. S.; Seo, J.; Yun, J. S.; Ho-Baillie, A.; Huang, S.; Green, M. A.; Seidel, J.; Ahn, T. K.; Seok, S. I. Beneficial Effects of PbI_2 Incorporated in Organo-Lead Halide Perovskite Solar Cells. *Adv. Energy Mater.* **2016**, *6*, 1502104.

(23) Liu, F.; Dong, Q.; Wong, M. K.; Djurišić, A. B.; Ng, A.; Ren, Z.; Shen, Q.; Surya, C.; Chan, W. K.; Wang, J.; Ng, A. M. C.; Liao, C.; Li, H.; Shih, K.; Wei, C.; Su, H.; Dai, J. Is Excess PbI_2 Beneficial for Perovskite Solar Cell Performance? *Adv. Energy Mater.* **2016**, *6*, 1502206.

(24) Gujar, T. P.; Unger, T.; Schönleber, A.; Fried, M.; Panzer, F.; van Smaalen, S.; Köhler, A.; Thelakkat, M. The role of PbI_2 in $CH_3NH_3PbI_3$ perovskite stability, solar cell parameters and device degradation. *Phys. Chem. Chem. Phys.* **2018**, *20*, 605−614.

(25) Yang, S.; Chen, S.; Mosconi, E.; Fang, Y.; Xiao, X.; Wang, C.; Zhou, Y.; Yu, Z.; Zhao, J.; Gao, Y.; De Angelis, F.; Huang, J. Stabilizing halide perovskite surfaces for solar cell operation with wide-bandgap lead oxysalts. *Science* **2019**, *365*, 473−478.

(26) Brumer, M.; Kigel, A.; Amirav, L.; Sashchiuk, A.; Solomesch, O.; Tessler, N.; Lifshitz, E. PbSe/PbS and $PbSe/PbSe_xS_{1-x}$ Core-Shell Nanocrystals. *Adv. Funct. Mater.* **2005**, *15*, 1111−1116.

(27) Lifshitz, E.; Brumer, M.; Kigel, A.; Sashchiuk, A.; Bashouti, M.; Sirota, M.; Galun, E.; Burshtein, Z.; Le Quang, A. Q.; Ledoux-Rak, I.; Zyss, J. Air-Stable PbSe/PbS and $PbSe/PbSe_xS_{1-x}$ Core-Shell Nanocrystal Quantum Dots and Their Applications. *J. Phys. Chem. B* **2006**, *110*, 25356−25365.

(28) Heyd, J.; Scuseria, G. E.; Ernzerhof, M. Erratum: Hybrid functionals based on a screened Coulomb potential [J. Chem. Phys. 118, 8207 (2003)]. *J. Chem. Phys.* **2006**, *124*, 219906.

(29) Kresse, G.; Furthmüller, J. Efficiency of ab-initio total energy calculations for metals and semiconductors using a plane-wave basis set. *Comput. Mater. Sci.* **1996**, *6*, 15−50.

(30) Nose, S. Constant temperature molecular dynamics methods. *Prog. Theor. Phys.* **1991**, *103*, 1−46.

https://dx.doi.org/10.1021/acsaem.0c02122
ACS Appl. Energy Mater. 2020, 3, 10328−10332